



Investigation of omnidirectional reflection band in ZnTe/ZnSe distributed Bragg reflector



Ying-Shin Huang^a, Sheng-Yao Hu^b, Yueh-Chien Lee^{c,*}, Chung-Cheng Chang^a, Kwong-Kau Tiong^a, Ji-Lin Shen^d, Wu-Ching Chou^e

^a Department of Electrical Engineering, National Taiwan Ocean University, Keelung 20224, Taiwan

^b Department of Digital Technology Design, Tungfang Design University, Kaohsiung 82941, Taiwan

^c Department of Electronic Engineering, Tungnan University, New Taipei City 22202, Taiwan

^d Department of Physics, Chung Yuan Christian University, Chung-Li 32023, Taiwan

^e Department of Electrophysics, National Chiao Tung University, Hsinchu 30010, Taiwan

ARTICLE INFO

Article history:

Received 8 June 2015

Received in revised form

19 July 2015

Accepted 20 July 2015

Available online 21 July 2015

Keywords:

ZnTe

ZnSe

Distributed Bragg reflectors

Reflectance

Molecular beam epitaxy

ABSTRACT

We report the characteristics of reflectance spectra of the 15- and 20-period ZnTe/ZnSe distributed Bragg reflector grown on GaAs (001) substrates by molecular beam epitaxy. The reflectance spectra measured at various incident angles and polarizations were investigated by the theoretical curves simulated using transfer matrix method. The wavelength variation of the refractive indices described by Sellmeier equation and random thickness model were also considered for the interpretation of the experimentally observed curves. An omnidirectional reflection range defined from the edge of incident-angle-dependent reflection band with TE and TM polarizations is about 15 nm, and is consistent with the observed experimental curves. The results showed that the selected ZnTe and ZnSe materials are suitable for constructing multilayer structures having omnidirectional reflection band.

© 2015 Elsevier B.V. All rights reserved.

1. Introduction

The distributed Bragg reflector (DBR) is a periodic multilayered structure which consists of two different materials with the high- and low-refractive indices, and the thickness of each layer is a quarter of the designed resonant wavelength of the stop-band. The high reflective performance of the stop-band of DBR can be achieved by selecting a large difference between the indices of refraction (Δn) of the two-layer materials and increasing the number of periods (N) in the DBR stack. The DBR structure has been widely applied in a variety of optoelectronic devices such as vertical-cavity surface emitting lasers (VCELs), Fabry–Perot modulators, and resonant cavity light emitting diodes (RCLEDs) [1–5].

The application of DBR can be promoted to operate as an omnidirectional reflector, where both transverse electric (TE) and transverse magnetic (TM) polarized waves at specific wavelength band can be reflected at all angles of incidence. It is also known that

the band edges of the omnidirectional reflectance band would be defined by the reflectance band for the propagation of TE and TM polarization at any incident angle in the periodic multilayered stack [6,7]. If a DBR originally designed for normal-incidence reflectance has an omnidirectional reflectance band, it can exhibit more advantages of lower optical loss and higher reflectivity, which should be useful in the fabrication of micro-cavities or coaxial waveguides [8,9].

In this work, the ZnTe and ZnSe materials with a large value of Δn (≈ 0.4) and suitable band gap energy are selected for fabricating the DBR structure for the resonant wavelength of 570 nm at the center of stop-band [10–12]. The reflectance spectra of 15- and 20-period ZnTe/ZnSe multilayer films prepared by molecular beam epitaxy (MBE) were measured at different angles of incidence for both polarization configurations (TE and TM) and compared with the theoretical simulation using the transfer matrix method. The omnidirectional reflection band derived from the variations in the resonant wavelength and width of reflectance band in terms of the incident angle for TE and TM polarizations is investigated and discussed.

* Corresponding author.

E-mail address: jacklee@mail.ntnu.edu.tw (Y.-C. Lee).

2. Experimental procedure

Fig. 1 shows the schematic diagram of ZnTe/ZnSe multilayer films. The stop-band center of ZnTe/ZnSe multilayer films is designed to be at 570 nm for application in the green–yellow spectrum. The assigned thicknesses (d_m) of ZnTe and ZnSe layers estimated from the relation $d_m = \frac{570}{4n_m}$ nm, with n_m ($n_{\text{ZnTe}} = 3.07$ and $n_{\text{ZnSe}} = 2.63$) being the refractive indices, were determined to be 46.4 and 54.2 nm, respectively. The detailed growth process for preparing 15- and 20-period ZnTe/ZnSe has been reported in previous work [13].

The reflectance spectra of ZnTe/ZnSe multilayer films were measured at different incident angles of 0, 15, 30, 45, 60, and 75° for TE- and TM-polarized light. The Xenon lamp was used as the light source and the reflected beam was dispersed through a 0.5 m spectrometer (Zolix omni- λ 500) with a grating of 1200 grooves/mm and detected by a photomultiplier tube.

3. Results and discussion

The reflectivity spectra of 15- and 20-period ZnTe/ZnSe multilayer films measured at normal incidence are shown as opened dots in Fig. 2 and Fig. 3, respectively. It can be observed that the stop-band center of the reflectivity spectrum of the 15- and 20-period ZnTe/ZnSe stacks is at about 576 and 582 nm with a maximum reflectivity of 91% and 98%, respectively. The results reflect the strong dependence of the performances of the DBR reflectance on the deposited number of periods. In the following, the deviated stop-band center and the undesired asymmetric shape of the reflectivity spectrum are presented and discussed.

In order to clarify the discrepancy between the theoretical and experimental spectra, a theoretical calculation based on the transfer matrix method has been carried out to compare the simulation curve with the experimental spectrum. The equation of the transfer matrix [14] is given by

$$\begin{pmatrix} M_{11} & M_{12} \\ M_{21} & M_{22} \end{pmatrix} = D_0^{-1} [D_H \cdot P_H \cdot D_H^{-1} \cdot D_L \cdot P_L \cdot D_L^{-1}]^N D_S \quad (1)$$

where N is the number of periods; $D_m = \begin{bmatrix} 1 & 1 \\ n_m & -n_m \end{bmatrix}$, $m = 0, H, L$ and S , are respectively the dynamic matrices for free space, ZnTe, ZnSe and GaAs (001) substrate; $P_m = \begin{bmatrix} e^{i\varphi_m} & 0 \\ 0 & -e^{i\varphi_m} \end{bmatrix}$, $m = H$ or L are the propagation matrices for ZnTe and ZnSe, respectively. The phase term φ_m is given by $\varphi_m = \frac{2\pi n_m d_m}{\lambda}$ where n_m and d_m are respectively, the refractive indices and thicknesses of ZnTe or ZnSe. The

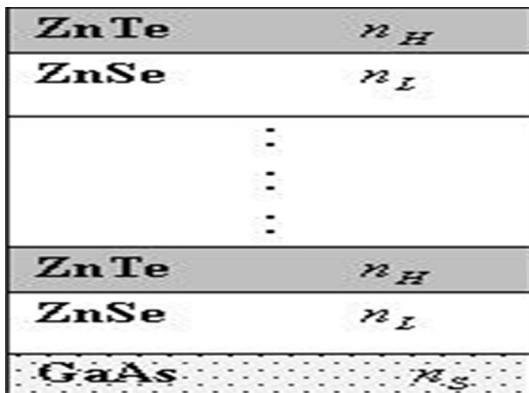


Fig. 1. Schematic diagram of ZnTe/ZnSe multilayer films.

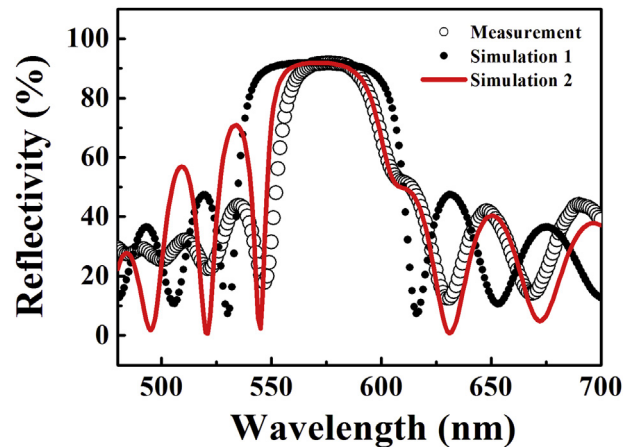


Fig. 2. Measured and simulated reflectance spectrum of the 15-period ZnTe/ZnSe multilayer films.

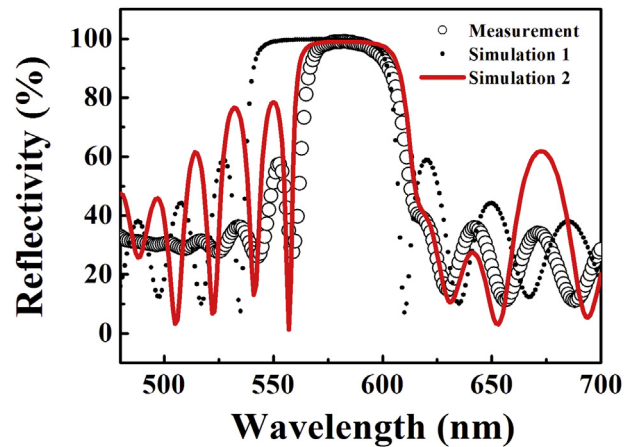


Fig. 3. Measured and simulated reflectance spectrum of the 20-period ZnTe/ZnSe multilayer films.

theoretical curves (simulation 1) are plotted as solid dots in Figs. 2 and 3. For the calculation of the simulation 1 curve, constant refractive indices of $n_{\text{ZnTe}} = 3.06$ and $n_{\text{ZnSe}} = 2.63$ together with the designed thicknesses of ZnTe and ZnSe were used. As can be observed, the curve of simulation 1 cannot describe well the measured spectra of the 15- and 20-period ZnTe/ZnSe stacks. The deviation indicates that the two important factors of refractive index and thickness of the layer as given in the transfer matrix equation have to be further considered.

The refractive index of the material is known to vary with wavelength. Therefore the wavelength-dependent refractive indices must be considered instead of the constant refractive index value. Accordingly, the Sellmeier equation [15] for the wavelength-dependent refractive indices of ZnTe and ZnSe as given by $n_{\text{ZnTe}} = \sqrt{3.96 + \frac{3.29 \times \lambda^2}{\lambda^2 - 0.366^2}}$ and $n_{\text{ZnSe}} = \sqrt{4.00 + \frac{1.90 \times \lambda^2}{\lambda^2 - 0.113^2}}$, respectively, are used in the transfer matrix equation. Furthermore, the unavoidable lattice mismatch (>7%) existing between the ZnTe and ZnSe layers would also result in the manifestation of 'waviness' of the individual layers [10]. These mean that the actual deposited ZnTe and ZnSe layers cannot attain the designed thicknesses in addition to the non-uniform interface. Murtaza and Campbell investigated the changes in layer thicknesses during a growth run on reflectivity spectra and presented a model for distributed

random thicknesses using a random number generator to generate modified thickness with a standard deviation [16]. Hence, the modified thickness with standard deviations of 9% and 8% of the designed thicknesses for ZnTe and ZnSe layer, respectively, were obtained according to this model. Successfully, the recalculated curves (simulation 2) shown as the red solid lines in Figs. 2 and 3, by taking account of the wave-dependent refractive indices and the distributed random thicknesses in the transfer matrix equation, can describe well the stop-band of the measured reflectivity spectra.

The reflectance spectrum of the 15- and 20-period ZnTe/ZnSe stacks at different incident angles of 0 (normal), 15, 30, 45, 60, 75° for TE and TM polarizations were measured and shown in Figs. 4 and 5. By increasing the incident angle, two considerable performances of the reflectance spectra should be further discussed. One is the stop-band center of the reflectance spectrum shifting toward shorter wavelengths, and the other one is the variation in the shape of the high reflectance band for TE and TM polarizations. The spectra exhibit increased TE bandwidth while the TM bandwidth decreases with increasing incident angle. It also shows the significant enhancement and reduction in the sharpness on the short-wavelength side of the high reflectance band for TE and TM polarizations, respectively. To compare the incident-angle-dependent reflectance spectrum, the effective dynamic and propagation matrices, including the factor of the incident angle θ , modified as

$$D_{TE} = \begin{bmatrix} 1 & 1 \\ n_m \cos \theta & -n_m \cos \theta \end{bmatrix} \quad \text{for TE polarization,}$$

$$D_{TM} = \begin{bmatrix} \cos \theta & -\cos \theta \\ n_m & n_m \end{bmatrix} \quad \text{for TM polarization, and}$$

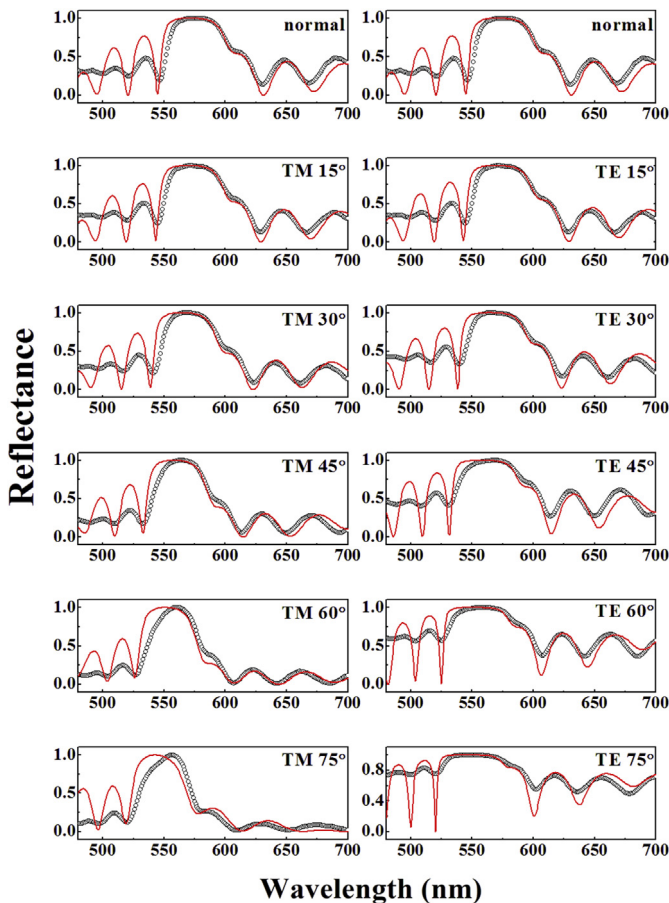


Fig. 4. Incident angle-dependent reflectance spectra of 15-period ZnTe/ZnSe multi-layer films for TM and TE polarizations.

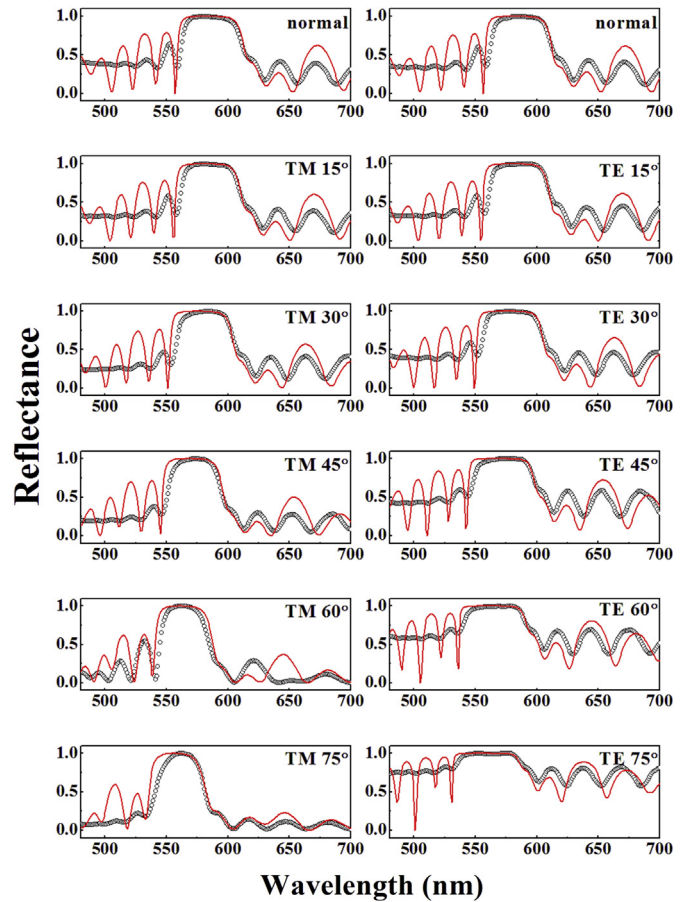


Fig. 5. Incident angle-dependent reflectance spectra of 20-period ZnTe/ZnSe multi-layer films for TM and TE polarizations.

$P_m = \begin{bmatrix} e^{i\varphi_m} & 0 \\ 0 & -e^{i\varphi_m} \end{bmatrix}$ with $\varphi_m = \frac{2\pi n_m d_m \cos \theta}{\lambda}$ [17,18] were substituted in Eq. (1). As shown in Figs. 4 and 5, the simulated curves utilizing the as described modification and displayed as the solid line can predicate clearly the variations in the shapes of the high reflectance band and are in good agreement with the measured reflectance spectra for all incident angles and polarizations.

Figs. 4 and 5 also show that there is an overlapping stop-band for both TE and TM polarizations at different incident angle, which has been represented as the omnidirectional reflectance band [6,7,19,20]. The omnidirectional reflectance band has been determined to depend on the index ratio of the stacked layers and the indices themselves should also be higher than (by > 1.5) that of the ambient [7]. Ideally, the index ratio, which determined the band splittings, should be higher than 1.5. In the current study, the fabricated DBR structure is for wide band gap application. Therefore the choice of materials may be quite limited. As listed earlier, we have $n_{ZnTe}/n_{ZnSe} = 1.163$ which is far lower than the value of 1.5 for good omnidirectional design. Nevertheless, the choice of ZnTe and ZnSe do satisfy the requirement that their refractive indices should be larger than the ambient by more than 1.5 to suppress the frequency of the Brewster crossing for the TM polarization [6,7]. The omnidirectional reflectance band is an important characteristic for designing DBR, and its performance directly depends on the variations of the band-edge wavelength λ_E of the reflectance spectra as a function of incident angle. The equation governing λ_E is given as [19]

$$\lambda_E = \lambda_C [1 \pm \Delta g] \quad (2)$$

where,

$$\lambda_C = \lambda_0 \left[\left(1 - \sin^2 \theta_0 / n_{ZnSe}^2 \right)^{1/2} + \left(1 - \sin^2 \theta_0 / n_{ZnTe}^2 \right)^{1/2} \right] \quad (3)$$

and

$$\Delta g = (2/\pi) \sin^{-1} [(\eta_H - \eta_L) / (\eta_H + \eta_L)] \quad (4)$$

The λ_C in Eq. (3) describing the center of the reflectance band as a function of incident angle is derived from the propagation angles differing in the high (n_{ZnTe}) and low (n_{ZnSe}) refractive index layers according to Snell's law [19,21]. The substituted θ_0 and λ_0 are the angle of incidence in incident medium assumed to be in air with $n_0 = 1$ and the resonant wavelength of reflectance band at normal incidence, respectively. The equation Δg , is modified from its usual normal-incidence definition to include the dependence on effective refractive indices (η_H or η_L) to account for the different polarization states [19]. The TE and TM effective refractive indices are given by $\eta_{TE} = [n_m^2 - \sin^2 \theta_i]^{1/2}$ and $\eta_{TM} = n_m^2 / [n_m^2 - \sin^2 \theta_i]^{1/2}$. Hence, for TE polarization, we can write $\eta_H = [n_{ZnTe}^2 - \sin^2 \theta_i]^{1/2}$ and $\eta_L = [n_{ZnSe}^2 - \sin^2 \theta_i]^{1/2}$ in Eq. (4). Similarly, η_H or η_L can also be derived for TM polarization.

From Eqs. (2)–(4), the theoretical TE- and TM-reflection bands in terms of wavelength and incident angle for 15- and 20-period samples are plotted in Figs. 6 and 7, respectively. The solid curves are the edges of TE-reflection band and the dashed curves are the TM-reflection band. It can be observed that the bandwidth of TE-reflection band increases, while that of TM-reflection band decreases as a function of incident angle. The observations are in good agreement with the experimental curves. From the longer-wavelength TM-reflection edge at incident angle of 90° and the shorter-wavelength TE-reflection edge at incident angle of 0°, we can deduce that the absolute omnidirectional reflectance band for the 15- and 20 period ZnTe/ZnSe multilayer films is about 15 nm and shown as the grey area in Figs. 6 and 7. For the experimental spectra of 15 and 20-period samples, the wavelength range for the omnidirectional reflectance band can be estimated from the measured reflectance results as depicted in Figs. (4) and (5). The overlapped stop band (defined for reflectance values larger than 0.75) for TE and TM polarizations with different incident angles is from 555 nm to 568 nm (bandwidth of 13 nm) for 15-period DBR

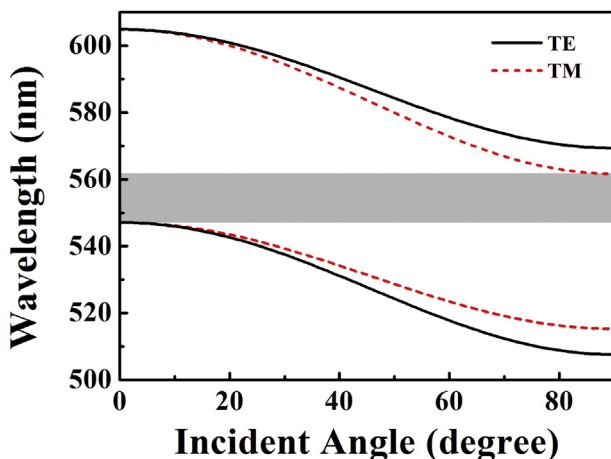


Fig. 6. Long- and short-wavelength reflection band edges of the 15-period ZnTe/ZnSe multilayer films for TE (solid line) and TM (dashed line) polarizations.

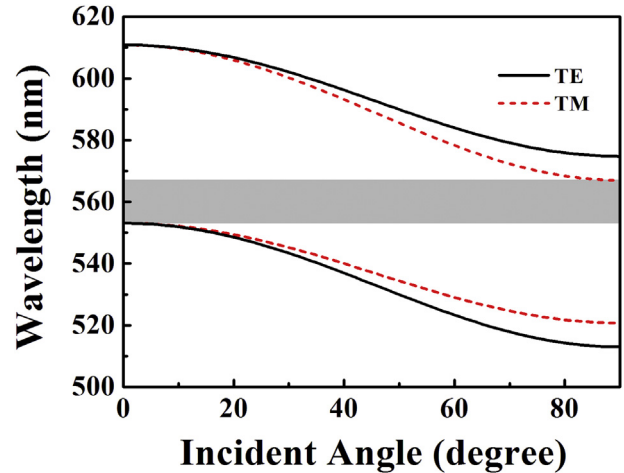


Fig. 7. Long- and short-wavelength reflection band edges of the 20-period ZnTe/ZnSe multilayer films for TE (solid line) and TM (dashed line) polarizations.

stack. The corresponding wavelength range is 564 nm–576 nm (bandwidth of 12 nm) for the 20-period sample. In general, the experimental results agreed reasonably well with that of the theoretical prediction.

4. Conclusion

In conclusion, we have investigated the reflectance spectra of the 15- and 20-period ZnTe/ZnSe multilayer films with incident-angle and polarization dependence. The transfer matrix method taken account of wavelength-dependent refractive index and distributed random thickness has been calculated to clarify the variations in the incident-angle-dependent reflectance spectra on TE or TM polarized light. An omnidirectional reflectance bandwidth, the high reflectance regime independent with the incident angle and polarized light, can be obtained as 15 nm for the 15- and 20-period ZnTe/ZnSe multilayer films, respectively. The results evidence that the ZnTe and ZnSe materials could be the favorable candidates for constructing the omnidirectional reflectors.

Acknowledgment

The authors would like to acknowledge the support of the Ministry of Science and Technology Project No. MOST 103-2633-E-236-001 and 102-2221-E-272 -006.

References

- [1] D.L. Huffaker, D.G. Deppe, Low threshold vertical-cavity surface-emitting lasers based on high contrast distributed Bragg reflectors, *Appl. Phys. Lett.* 70 (1997) 1781–1783.
- [2] C. Roux, E. Hadji, J.L. Pauarat, Room-temperature optically pumped CdHgTe vertical-cavity surface-emitting laser for the 1.5 μm range, *Appl. Phys. Lett.* 75 (1999) 1661–1663.
- [3] M.Y. Liu, S.Y. Chou, High-modulation-depth and short-cavity-length silicon Fabry–Perot modulator with two grating Bragg reflectors, *Appl. Phys. Lett.* 68 (1996) 170–172.
- [4] E.F. Schubert, Y.H. Wang, A.Y. Cho, L.W. Tu, G.J. Zydzik, Resonant cavity light-emitting diode, *Appl. Phys. Lett.* 60 (1992) 921–923.
- [5] J.H. Kim, S.J. Lee, S.H. Park, InGaN-based resonant-cavity light-emitting diodes with a ZrO₂/SiO₂ distributed Bragg reflector and metal reflector, *Jpn. J. Appl. Phys.* 49 (2010) 122102.
- [6] Y. Fink, J.N. Winn, S. Fan, C. Chen, J. Michel, J.D. Joannopoulos, E.L. Thomas, A dielectric omnidirectional reflector, *Science* 27 (1998) 1679–1682.
- [7] J.N. Winn, Y. Fink, S. Fan, J.D. Joannopoulos, Omnidirectional reflection from a one-dimensional photonic crystal, *Opt. Lett.* 23 (1998) 1573–1575.
- [8] K.M. Chen, A.W. Sparks, H.C. Luan, D.R. Lim, K. Wada, L.C. Kimerling, SiO₂/TiO₂ omnidirectional reflector and microcavity resonator via the sol-gel method,

- Appl. Phys. Lett. 75 (1999) 3805–3807.
- [9] M. Ibanescu, Y. Fink, S. Fan, E.L. Thomas, J.D. Joannopoulos, An all-dielectric coaxial waveguide, *Science* 289 (2000) 415–419.
- [10] F.C. Peiris, S. Lee, U. Bindley, J.K. Furdyna, Molecular-beam-epitaxy-grown ZnSe/ZnTe high-reflectivity distributed Bragg reflectors, *Semicond. Sci. Technol.* 14 (1999) 878–882.
- [11] R. Sharma, N.S. Saxena, S. Kumar, T.P. Sharma, Optical band gap studies on ZnTe pellets, *Indian J. Pure Appl. Phys.* 44 (2006) 192–195.
- [12] S. Venkatachalam, Y.L. Jeyachandran, P. Sureshkumar, A. Dhayalraj, D. Mangalaraj, Sa.K. Narayandass, S. Velumani, Characterization of vacuum-evaporated ZnSe thin films, *Mater. Charact.* 58 (2007) 794–799.
- [13] C.B. Fu, C.S. Yang, M.C. Kuo, Y.J. Lai, J. Lee, J.L. Shen, W.C. Chou, S. Jeng, High reflectance ZnTe/ZnSe distributed Bragg reflector at 570 nm, *Chin. J. Phys.* 41 (2003) 535–543.
- [14] J.L. Shen, C.Y. Chang, P.N. Chen, W.C. Chou, Y.F. Chen, M.C. Wu, Optical absorption studies in absorbing Bragg reflectors, *Opt. Commun.* 199 (2001) 155–159.
- [15] H.H. Li, Refractive index of ZnS, ZnSe, and ZnTe and its wavelength and temperature derivatives, *J. Phys. Chem. Ref. Data* 13 (1984) 103–150.
- [16] S.S. Murtaza, J.C. Campbell, Effects of variations in layer thicknesses on the reflectivity spectra of semiconductor Bragg mirrors, *J. Appl. Phys.* 77 (1995) 3641–3644.
- [17] P. Yeh, *Optical Waves in Layered Media*, Wiley, New York, 1988, p. 109.
- [18] Y.S. Huang, S.Y. Hu, C.C. Huang, Y.C. Lee, J.W. Lee, C.C. Chang, Z.K. Wun, K.K. Tiong, Incident-angle-dependent reflectance in distributed Bragg reflectors fabricated from ZnO/MgO multilayer films, *Opt. Rev.* 21 (2014) 651–654.
- [19] W.H. Southwell, Omnidirectional mirror design with quarter-wave dielectric stacks, *Appl. Opt.* 38 (1999) 5464–5467.
- [20] D.N. Chigrin, A.V. Lavrinenko, D.A. Yarotsky, S.V. Gaponenko, Observation of total omnidirectional reflection from a one-dimensional dielectric lattice, *Appl. Phys. A* 68 (1999) 25–28.
- [21] V. Kumar, A. Kumar, K.H.S. Singh, P. Kumar, Broadening of omni-directional reflection range by cascade 1D photonic crystal, *Optoelectron. Adv. Mater. Rapid Commun.* 5 (2011) 488–490.